

**Structure and evolutionary trace-assisted screening of a residue swapping the substrate ambiguity and chiral specificity in an esterase**

Cea-Rama, Isabel; Coscolín, Cristina; Katsonis, Pangiotis; Bargiela, Rafael; Golyshin, Peter; Lichtarge, Olivier; Ferrer, Manuel; Sanz-Aparicio, Julia

**Computational and Structural Biotechnology Journal**

DOI:

[10.1016/j.csbj.2021.04.041](https://doi.org/10.1016/j.csbj.2021.04.041)

Published: 01/01/2021

Peer reviewed version

[Cyswllt i'r cyhoeddiad / Link to publication](#)

*Dyfyniad o'r fersiwn a gyhoeddwyd / Citation for published version (APA):*

Cea-Rama, I., Coscolín, C., Katsonis, P., Bargiela, R., Golyshin, P., Lichtarge, O., Ferrer, M., & Sanz-Aparicio, J. (2021). Structure and evolutionary trace-assisted screening of a residue swapping the substrate ambiguity and chiral specificity in an esterase. *Computational and Structural Biotechnology Journal*, 19, 2307-2317. <https://doi.org/10.1016/j.csbj.2021.04.041>

**Hawliau Cyffredinol / General rights**

Copyright and moral rights for the publications made accessible in the public portal are retained by the authors and/or other copyright owners and it is a condition of accessing publications that users recognise and abide by the legal requirements associated with these rights.

- Users may download and print one copy of any publication from the public portal for the purpose of private study or research.
- You may not further distribute the material or use it for any profit-making activity or commercial gain
- You may freely distribute the URL identifying the publication in the public portal ?

**Take down policy**

If you believe that this document breaches copyright please contact us providing details, and we will remove access to the work immediately and investigate your claim.

## Structure and evolutionary trace-assisted screening of a residue swapping the substrate ambiguity and chiral specificity in an esterase

Isabel Cea-Rama<sup>a, 1</sup>, Cristina Coscolín<sup>b, 1</sup>, Panagiotis Katsonis<sup>c</sup>, Rafael Bargiela<sup>d</sup>, Peter N. Golyshin<sup>d,e</sup>, Olivier Lichtarge<sup>c</sup>, Manuel Ferrer<sup>b,\*</sup>, and Julia Sanz-Aparicio<sup>a,\*</sup>

<sup>a</sup>*Institute of Physical Chemistry "Rocasolano", CSIC, 28006 Madrid, Spain*

<sup>b</sup>*Institute of Catalysis, CSIC, 28049 Madrid, Spain*

<sup>c</sup>*Baylor College of Medicine, Houston, TX 77030, USA*

<sup>d</sup>*Centre for Environmental Biotechnology, Bangor University, LL57 2UW Bangor, UK*

<sup>e</sup>*School of Natural Sciences, Bangor University, LL57 2UW Bangor, UK*

<sup>1</sup>These authors contributed equally to this work.

\*Corresponding authors at: Institute of Physical Chemistry "Rocasolano", CSIC, Serrano 119, 28006 Madrid, Spain (J. Sanz-Aparicio). Institute of Catalysis, CSIC, Marie Curie 2, 28049 Madrid, Spain (M. Ferrer).

*E-mail addresses:* xjulia@iqfr.csic.es (J. Sanz-Aparicio), mferrer@icp.csic.es (M. Ferrer)

*Phone numbers:* +34915619400 (J. Sanz-Aparicio), +34915854872 (M. Ferrer)

Abbreviations:  $E_{app}$ , apparent enantioselectivity; ET, evolutionary trace; EA, evolutionary action; HEPES, 40 mM 4-(2-hydroxyethyl)-1-piperazineethanesulfonic acid; Ni-NTA, nickel-nitrilotriacetic acid.

Short title: Tracing position swapping specificity

## 1 ABSTRACT

2  
3 Our understanding of enzymes with high substrate ambiguity remains limited because their  
4 large active sites allow substrate docking freedom to an extent that seems incompatible with  
5 stereospecificity. One possibility is that some of these enzymes evolved a set of  
6 evolutionarily fitted sequence positions that stringently allow switching substrate ambiguity  
7 and chiral specificity. To explore this hypothesis, we targeted for mutation a serine ester  
8 hydrolase (EH<sub>3</sub>) that exhibits an impressive 71-substrate repertoire but is not stereospecific  
9 (*e.e.* 50%). We used structural actions and a computational approach, the evolutionary trace  
10 method, to explore specificity-swapping sequence positions and hypothesized that position  
11 I244 was critical. Driven by evolutionary action analysis, this position was substituted to  
12 leucine, which together with isoleucine appears to be the amino acid most commonly  
13 present in the closest homologous sequences (max. identity, *ca.* 67.1%), and to  
14 phenylalanine, which appears in distant homologues. While the I244L mutation did not have  
15 any functional consequences, the I244F mutation allowed the esterase to maintain a  
16 remarkable 53-substrate range while gaining stereospecificity properties (*e.e.* 99.99%).  
17 These data support the possibility that some enzymes evolve sequence positions that  
18 control the substrate scope and stereospecificity. Such residues, which can be evolutionarily  
19 screened, may serve as starting points for further designing substrate-ambiguous but chiral-  
20 specific enzymes that are greatly appreciated in biotechnology and synthetic chemistry.

21  
22 Keywords: crystal structure; esterase; evolutionary trace; promiscuity; protein engineering;  
23 specificity.

## 24 25 1. Introduction

26  
27 The pivotal assets provided by the use of enzymes in industrial processes and consumer  
28 products include the following: a lower energy footprint; reduced waste production and  
29 chemical consumption; safer process conditions; and the use of renewable feedstocks. As  
30 such, replacing chemicals (including chemical catalysts) with enzymes in industrial processes  
31 or consumer products is expected to positively impact greenhouse gas emissions (reported  
32 savings from 0.3 to 990 kg CO<sub>2</sub> equivalent/kg product) and global warming issues by  
33 reducing water and energy consumption (estimates: 6000 million m<sup>3</sup> and 167 TWh,  
34 respectively) [1]. In particular, enzymes with broad substrate ambiguity and exact stereo-  
35 control are appreciated as candidates for developing alternative methods to conventional  
36 chemical catalysis in bench work and the pharmaceutical industry [2,3]. However, enzymes  
37 that combine both features are rare. Indeed, most enzymes designed by nature through four  
38 billion years of evolution perform primary reactions with exquisite specificity [4]. The  
39 universe of enzymes with ambiguous specificities is also large, but the voluminous active  
40 sites selected in evolution to provide a high level of substrate docking freedom are  
41 commonly not stereospecific [5], which limits the technological potential of multi-specific (or  
42 substrate-ambiguous) enzymes. A better understanding of how substrate specificity can be  
43 modulated in such enzymes would assist engineering strategies [6] in increasing their  
44 technological impact.

45 Past studies have shown that enzyme specificity is influenced by the architecture (size  
46 and geometry) of their active-site cavity and by their access tunnels [7], which can evolve  
47 from an ancestral core domain or a minimal structural unit within a superfamily [8]. In

48 general, large active sites are consistent with the very broad substrate specificity of these  
49 enzymes, whereas enzymes with smaller and occluded cavities cannot readily accommodate  
50 a larger number of substrates [7,9]. Aside from these general trends, the presence of key  
51 substitutions in the active site and in the access tunnels [10,11] or the positioning of water  
52 molecules [12] or anions [13] in the proximity of the active site may influence the entrance  
53 and positioning of certain substrates. In other cases, alterations in specificity were ascribed  
54 to large structural elements that are inserted, removed or rearranged in the sequence [14]  
55 or to differences in the protein dynamics [15]. Few substitutions were also found to be  
56 sufficient to modify the reaction mechanisms of enzymes, which opens the possibility to  
57 transform distinct molecules [16]. These studies exemplify that influencing and expanding  
58 the substrate specificity of enzymes is feasible. Prominent examples with remarkable  
59 substrate specificity are the human cytochrome P450 enzyme [17] and resurrected TEM-1  $\beta$ -  
60 lactamases [18]. The application of multiple engineering methodologies has also  
61 demonstrated that the transformation of a nonspecific enzyme into a specific enzyme is also  
62 theoretically feasible [11,19-22], with this transformation being more effective when altering  
63 residues close to the active site or the substrate accessibility channel [23,24].

64 While modulating substrate specificity in enzymes is thus feasible when examined as  
65 separate properties, introducing chiral specificity to an enzyme with prominent substrate  
66 ambiguity is challenging and has received much less attention. Few examples have been  
67 reported, such as engineered horseradish peroxidase [25], cytochrome CYP3A4 [26],  
68 peroxidase C45 [27], Michaelase [28], beta-lactamases [29] or esterase [30], which showed  
69 chiral specificity while having moderate substrate ambiguity; however, in most cases,  
70 specificity was established on the basis of a limited set of structurally similar substrates.

71 Here, we exploit previous comprehensive information on the substrate specificity of a  
72 large set of ester hydrolases [9] tested with close to one hundred distinct esters to identify  
73 one such enzyme, EH<sub>3</sub>, which has remarkable multi-specificity, with sequence positions that  
74 modulate both substrate ambiguity and chiral specificity. We focused on carboxylic ester  
75 hydrolases (EC 3.1.1), as they are among the most important biocatalysts in the field of  
76 biotechnology [31], and because of their capacity to catalyze hydrolysis with exquisite  
77 enantio-, regio-, and stereospecificity. According to their sequence, they are grouped into 19  
78 different families with more than 1,500 available protein structures according to the lipase  
79 engineering database [32]. Through this investigation, we asked the following questions: Are  
80 there sequence positions that determine enzyme specificity? Can these positions be  
81 screened and used to produce substrate-promiscuous but chiral-specific enzymes?  
82 Answering these questions may be fundamental from a basic point of view. Thus, functional  
83 residues in enzymes tend to be highly conserved over evolution [33,34], but to what extent  
84 certain sites impose substrate ambiguity over chiral specificity and, conversely, their  
85 conservation through evolution are not known. This is of special significance given that  
86 genome-scale model simulations and laboratory evolution experiments have shown that few  
87 mutations shift enzyme substrate turnover rates toward new substrates, thus shaping  
88 microbial adaptation to novel growth substrates [35]. From a technological point of view,  
89 answering these questions will also have implications for fine-tuning enzyme specificity. For  
90 the purpose of this study, we herein explore the evolutionary importance of sequence  
91 positions that possibly have functional roles in the chiral specificity of substrate ambiguous  
92 esterase through the application of a software program called Evolutionary Trace [36,37]  
93 and structure-assisted and experimental validations. We would like to highlight that previous  
94 work on evolutionary traces [38] focused on altering the substrate specificity for a few

95 substrates, and to the best of our knowledge, their application to modulate enzyme  
96 specificity in combination with substrate promiscuity has not yet been reported.

97

## 98 **2. Materials and methods**

99

### 100 *2.1. Enzyme source, production and purification*

101 The vector pBXNH3 and the host *Escherichia coli* MC1061 were the sources of His<sub>6</sub>-tagged  
102 EH<sub>3</sub> (GenBank acc. nr. KY483645), a serine ester hydrolase isolated from the metagenomic  
103 DNA of microbial communities inhabiting the chronically polluted seashore area of Milazzo  
104 Harbor in Sicily [9]. The soluble His-tagged protein was produced and purified at 4°C after  
105 binding to a Ni-NTA His-Bind resin (from Merck Life Science S.L.U., Madrid, Spain) as  
106 described previously [39]. The purity was assessed as >98% using SDS-PAGE analysis in a  
107 Mini PROTEAN electrophoresis system (Bio-Rad, Madrid, Spain). Purified protein was stored  
108 at -86°C until use at a concentration of 10 mg ml<sup>-1</sup> in 40 mM 4-(2-hydroxyethyl)-1-  
109 piperazineethanesulfonic acid (HEPES) buffer (pH 7.0). A total of approximately 20 mg of  
110 total purified recombinant protein was obtained from a 1-liter culture.

111

### 112 *2.2. Source of chemicals*

113 The source or brand for each of the esters [purity ≥99%] used in this study has been  
114 described previously [9]. Methyl-(*R*)-2-phenylpropanoate and methyl-(*S*)-2-  
115 phenylpropanoate [purity ≥99%] were purchased from Combi-Blocks (San Diego, CA, USA).  
116 HEPES [purity ≥99%] was purchased from Fisher Bioreagent (Ottawa, ON, USA). All other  
117 chemicals [with the highest purity available] were purchased from Merck Life Science S.L.U.,  
118 Madrid, Spain) and Sigma-Aldrich Química S.A. Madrid (Spain).

119

### 120 *2.3. Crystallization and X-ray structure determination of EH<sub>3</sub> complexed with methyl-(*R/S*)-2-phenylpropanoate*

122 The crystallization conditions reported for the native protein were optimized by  
123 adjusting the protein and precipitant concentrations. The best crystals were grown by using  
124 1 μl of EH<sub>3S192A</sub> (20-60 mg ml<sup>-1</sup> in 40 mM HEPES (pH 7) and 100 mM NaCl) and 0.5 μl of  
125 precipitant solution (28-29% PEG3000, 0.1 M Bis-tris (pH 6.5), and 0.2 M MgCl<sub>2</sub>·6H<sub>2</sub>O). The  
126 complexes were obtained by soaking thin plate-shaped crystals of EH<sub>3S192A</sub> in mother liquor  
127 supplemented with 10-20 mM methyl-(*S/R*)-2-phenylpropanoate for 1-3 hours. For data  
128 collection, crystals were transferred to cryoprotectant solutions consisting of mother liquor  
129 plus 20-23% (v/v) glycerol before being cooled in liquid nitrogen. Diffraction data were  
130 collected using synchrotron radiation on the XALOC beamline at ALBA (Cerdanyola del  
131 Vallés, Spain). Diffraction images were processed with XDS [40] and merged using AIMLESS  
132 [41] from the CCP4 package [42]. Both crystals were indexed in the C2 space group, with two  
133 molecules in the asymmetric unit and 40% solvent content within the unit cell. The data  
134 collection statistics are given in **Table S1**.

135

136 The structure of the complex was solved by difference Fourier synthesis using the  
137 coordinates of the EH<sub>3</sub> native crystals (PDB ID: 6SXP). Crystallographic refinement was  
138 performed using the program REFMAC [43] within the CCP4 suite with local  
139 noncrystallographic symmetry (NCS). The free R-factor was calculated using a subset of 5%  
140 randomly selected structure-factor amplitudes that were excluded from the automated  
141 refinement. At the later stages, ligands were manually built into the electron density maps  
142 with Coot [44], and water molecules were included in the model, which, when combined  
with more rounds of restrained refinement, reached the R factors listed in **Table S1**. For

143 methyl-(*R/S*)-2-phenylpropanoate, which is not present in the Protein Data Bank, a model  
144 was built using MacPyMOLX11Hybrid (the PyMOL Molecular Graphics System, Version 2.0,  
145 Schrödinger, LLC). The model was used to automatically generate coordinates and molecular  
146 topologies with eLBOW [45], which is suitable for REFMAC refinement. The figures were  
147 generated with PyMOL. The crystallographic statistics of EH<sub>3S192A</sub> complexed with methyl-  
148 (*R/S*)-2-phenylpropanoate are listed in **Table S1**.

149

#### 150 2.4. Site-directed mutagenesis

151 Mutagenic PCR was performed using the QuikChange Lightning Multi Site-Directed  
152 Mutagenesis Kit (Agilent Technologies, Cheadle, UK), as described previously [22]. The  
153 forward primers used to generate the EH<sub>3I244L</sub> and EH<sub>3I244F</sub> variants were as follows: 5'-  
154 GCGAAAACAATGGCCTCATGATTGAACTGCATAAC-3' and 5'-  
155 GCGAAAACAATGGCTTCATGATTGAACTGCATAAC-3', respectively. The pBXNH3 plasmid  
156 containing EH<sub>3</sub> DNA [9] was used as a template to perform mutagenic PCR.

157

#### 158 2.5. Hydrolytic activity assessment

159 Ester hydrolysis was assayed using a pH indicator assay in 384-well plates at 30°C and pH  
160 8.0 in a Synergy HT Multi-Mode Microplate Reader in continuous mode at 550 nm over 24  
161 hours. Conditions were as detailed previously [39]. For  $K_m$  determination, [protein]: 4.5  $\mu\text{g}$   
162  $\text{ml}^{-1}$ ; [ester]: 0-100 mM; reaction volume: 44  $\mu\text{l}$ ; T: 30°C; and pH: 8.0. For  $k_{\text{cat}}$  determination,  
163 [protein]: 0-270  $\mu\text{g}$   $\text{ml}^{-1}$ ; [ester]: 50 mM; reaction volume: 44  $\mu\text{l}$ ; T: 30°C; and pH: 8.0.

164 The effect of pH on the activity was determined in 50 mM Britton and Robinson buffer  
165 at pH 4.0–12.0, following the production of 4-nitrophenol from the hydrolysis of 4-  
166 nitrophenyl-propionate ( $p\text{NPC}_3$ : 0.8 mM) at 348 nm ( $\epsilon = 4147 \text{ M}^{-1} \text{ cm}^{-1}$ ) over 5 min and  
167 determining the absorbance per minute from the slopes generated [22]. Reactions,  
168 performed at 30°C, each contained 2  $\mu\text{g}$  of protein in a total volume of 200  $\mu\text{l}$ . Similar assay  
169 conditions were used to assay the effects of temperature on esterase hydrolysis of  $p\text{NPC}_3$ ,  
170 but in this case, reactions were performed in 50 mM Britton and Robinson buffer pH 8.0.

171 All values, in triplicate, were corrected for nonenzymatic transformation. The absence of  
172 activity was defined as at least a twofold background signal as described [39].

173

#### 174 2.6. Hydrolysis of methyl-(*R/S*)-2-phenylpropanoate and gas chromatography (GC) analysis

175 Prior to the use of the racemic mixture, the continuous hydrolysis of separate methyl (*R*)-  
176 2-phenylpropanoate and methyl (*S*)-2-phenylpropanoate was performed. Briefly, 2  $\mu\text{l}$  of  
177 each enantiomer (from a stock solution of 200  $\text{mg}$   $\text{ml}^{-1}$  in acetonitrile) was added to 96  $\mu\text{l}$  of  
178 5 mM 4-(2-hydroxyethyl)-1-piperazinepropanesulfonic acid (EPPS) buffer (pH 8.0) containing  
179 0.9 mM Phenol Red (Merck Life Science S.L.U., Madrid, Spain). Then, 2  $\mu\text{l}$  of enzyme solution  
180 (from a stock solution of 1.0  $\text{mg}$   $\text{ml}^{-1}$  in 40 mM HEPES buffer, pH 7.0) was added, and the  
181 progress of the reaction at 30°C was followed continuously at 590 nm. These reaction  
182 conditions were set up to evaluate the chiral specificity using a racemic ester of methyl  
183 (*R/S*)-2-phenylpropanoate. After 60 min, reactions with racemic mixtures were stopped by  
184 adding 1800  $\mu\text{l}$  of HPLC-grade methanol, and the reaction products were analyzed by GC  
185 through a GC-Column CP-Chirasil-Dex CB (25 m length, 0.25  $\mu\text{m}$  internal diameter, 0.25  $\mu\text{m}$   
186 film) (Agilent J&W GC Columns), as previously described [22].

187

#### 188 2.7. Circular dichroism to estimate the thermal denaturation of EH<sub>3</sub>

189 Circular dichroism (CD) spectra were acquired between 190 and 270 nm with a Jasco J-  
190 720 spectropolarimeter equipped with a Peltier temperature controller, employing a 0.1-mm  
191 cell at 25°C. Spectra were analyzed, and denaturation temperature ( $T_d$ ) values were  
192 determined at 220 nm between 10 and 85°C at a rate of 30°C per hour in 50 mM Britton and  
193 Robinson buffer at pH 8.5. A protein concentration of 1.0 mg ml<sup>-1</sup> was used.  $T_d$  (and standard  
194 deviation of the linear fit) was calculated by fitting the ellipticity (mdeg) at 220 nm at each of  
195 the different temperatures using a 5-parameter sigmoid fit with SigmaPlot 13.0.

196

### 197 *2.8. Cavity volume and solvent-accessible surface area (SASA) calculation*

198 The relative solvent-accessible surface area (SASA) of the active site, computed as a  
199 (dimensionless) percentage of the ligand SASA in solution, was obtained using the GetArea  
200 web server [46]. Note that the relative SASA of the catalytic triad (derived from the GetArea  
201 server) adopts values of 0–100. The volume of the active site cavity was computed with  
202 fpocket [47], which is a very fast open-source protein pocket (cavity) detection algorithm  
203 based on Voronoi tessellation. fpocket includes two other programs (dpocket and tpocket)  
204 that allow the extraction of pocket descriptors and the testing of owned scoring functions,  
205 respectively.

206

### 207 *2.9. Evolutionary trace and evolutionary action computations*

208 The evolutionary importance of sequence positions was estimated using the *Evolutionary*  
209 *Trace (ET) method* [36,37], which is available at <http://lichtargelab.org/software/ETserver>.  
210 ET scores the functional importance of protein sequence positions by quantifying the  
211 correlation of variations in homologous proteins with the phylogenetic divergence of the  
212 sequences. Residue variations associated with large phylogenetic distances indicate  
213 important residues, and vice versa. The ET output is given as a top-ranked score (on the  
214 scale of 0 for the most important to 100 for the least important residues), which indicates  
215 the percentage of protein residues that were found to be more important than the residue  
216 of interest.

217 The functional impact of the potential amino acid substitutions was estimated using the  
218 *Evolutionary Action (EA) method* [48], which is available at <http://eaction.lichtargelab.org/>.  
219 EA estimates the evolutionary impact of sequence changes through a simple model of  
220 protein evolution that accounts for the evolutionary importance of the residue (ET method)  
221 and for the similarity of the substitution. The similarity of the substitution is quantified  
222 through substitution odds that are specific to the evolutionary importance, secondary  
223 structure, and solvent accessibility of each residue. The outcome is a rank score that  
224 indicates the percentage of all potential amino acid changes in the protein that are predicted  
225 to have less impact than the substitution of interest. Therefore, EA is given on a scale from 0  
226 (fully neutral) to 100 (fully deleterious).

227 Both ET and EA are required as inputs to provide an alignment of homologous sequences.  
228 We generated the input alignment using the default parameters of the ET server (UniRef90,  
229 20% minimum sequence identity, 0.5 minimum fractional length to query), which resulted in  
230 410 homologous sequences.

231

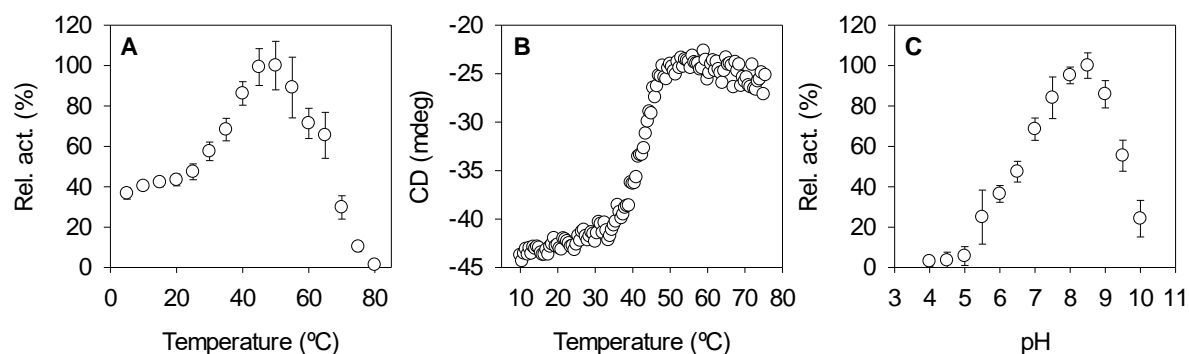
## 232 **3. Results and Discussion**

233

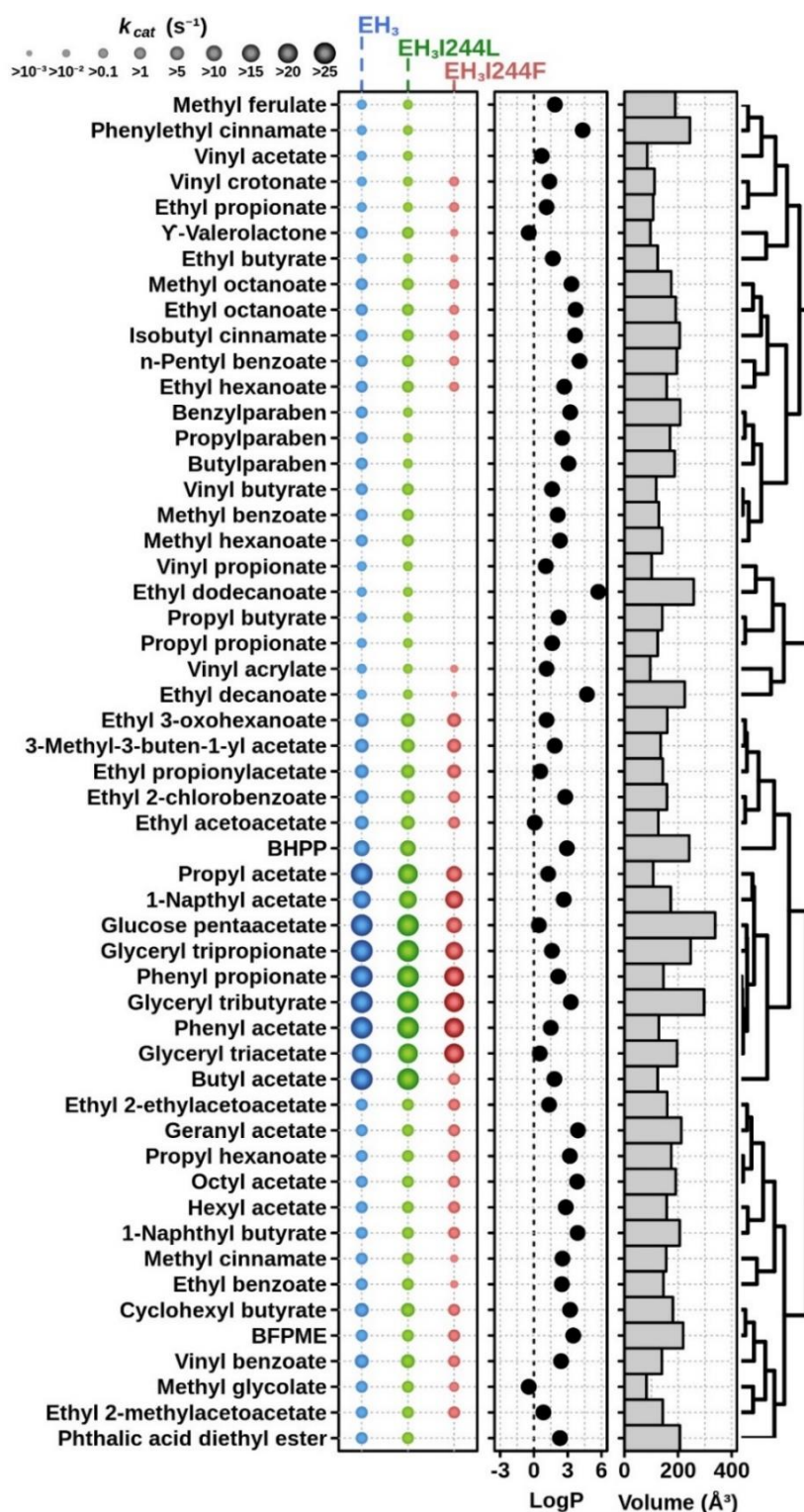
### 234 *3.1. Biochemical and substrate specificity characteristics of EH<sub>3</sub>*

235 EH<sub>3</sub> was identified in a recent study as the third most substrate-ambiguous ester hydrolase  
236 out of 145 tested enzymes [9]. This enzyme, which belongs to family IV of the Arpigny and  
237 Jaeger classification [31], originated from an uncultured bacterium of the genus  
238 *Hyphomonas* (phylum *Proteobacteria*), a highly versatile group of halophiles in terms of their  
239 ability to successfully grow in a variety of environmental conditions and capable of  
240 mineralizing a high number of pollutants [49]; this may be in agreement with the fact that  
241 this enzyme was isolated from a chronically polluted seashore area [9].

242 EH<sub>3</sub> did show maximal activity at 50°C, retaining more than 80% of the maximum activity  
243 at 40-55°C (**Fig. 1A**), suggesting that it is moderately thermostable. This was confirmed by  
244 circular dichroism analysis, which revealed a denaturing temperature of 45.90 ± 0.43°C (**Fig.**  
245 **1B**). Its optimal pH for activity is 8.5 (**Fig. 1C**). Its voluminous (volume of the active site  
246 cavity: 1718.02 Å<sup>3</sup>) but low exposed (solvent accessible surface area (SASA): 6.03 over 100  
247 dimensionless percentage) active site allows hydrolysis of a broad range of 71 structurally  
248 and chemically diverse esters, including non-chiral (**Fig. 2**) and chiral (**Fig. 3**) esters. Such  
249 topology, namely, active site cavities with large volume but low exposition to the surface,  
250 has been found to be beneficial for retaining a higher number of substrates in specific  
251 catalytic binding interactions and thus for promoting substrate promiscuity [9]. However, it  
252 is not stereospecific according to the quick apparent enantioselectivity ( $E_{app}$ ) method [50], in  
253 which the ratios between the  $k_{cat}/K_m$  of the preferred chiral ester and the nonpreferred  
254 chiral ester (from *ca.* 1.02 to 6.93; **Table 1**) were calculated when tested separately.

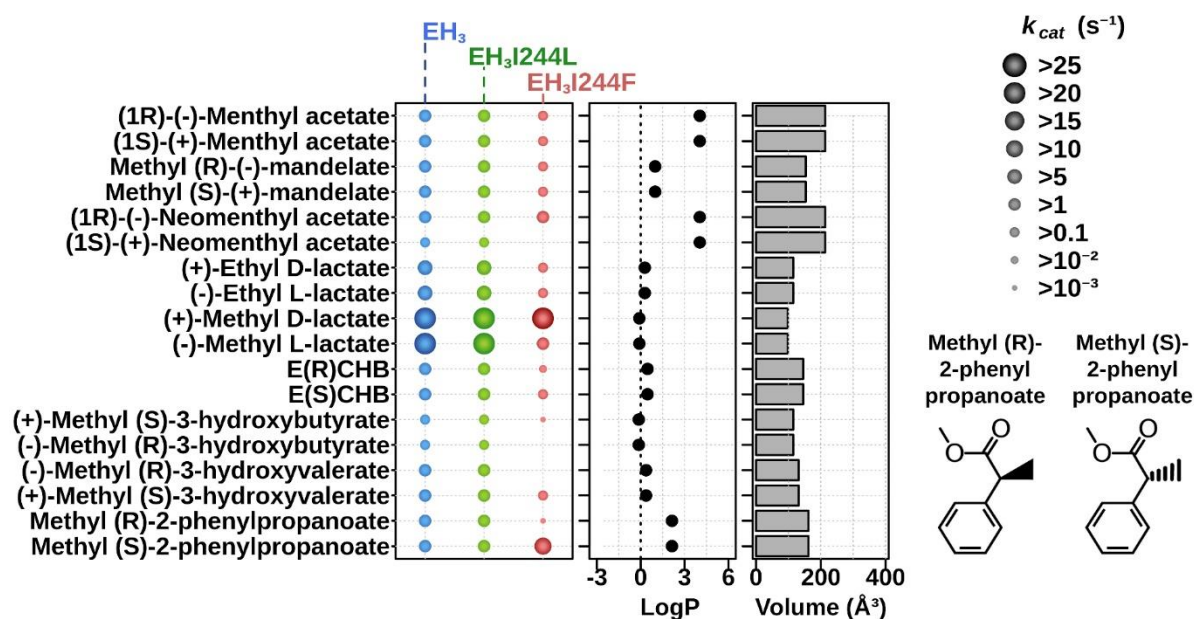


255 **Fig. 1.** Optimal parameters for the activity and stability of purified EH<sub>3</sub>. (A) Temperature  
256 profile determined as follows: protein, 2 µg; [*p*-nitrophenyl propionate (*pNPC*<sub>3</sub>)], 0.8 mM;  
257 pH, 50 mM Britton and Robinson buffer pH 8.0; T, 5-80°C; reaction volume, 200 µl. (B) The  
258 thermal denaturation curve of EH<sub>3</sub> at pH 7.0 was measured by ellipticity changes at 220 nm  
259 and obtained at different temperatures. (C) The pH profile was determined as follows:  
260 protein, 2 µg; [*pNPC*<sub>3</sub>], 0.8 mM; T, 30°C; pH, 50 mM Britton and Robinson buffer from 4.0 to  
261 10.0; reaction volume, 200 µl. Graphics were created with SigmaPlot version 14.0. The data  
262 are not fitted to any model.  
263  
264  
265



266  
 267 **Fig. 2.** Non-chiral substrate specificity. The  $k_{cat}$  ( $s^{-1}$ ) values of the EH<sub>3</sub>, EH<sub>3</sub>I244L and EH<sub>3</sub>I244F  
 268 variants were measured for 53 non-chiral carboxylic esters found to be hydrolyzed by any of  
 269 the enzyme variants. The substrates, with the hydrophobicity (log P) and volume (Å<sup>3</sup>)  
 270 indicated (details in **Table S2**), are ranked based on hierarchical clustering according to  
 271 substrate similarity profiles. For  $k_{cat}$  determination, calculated on a continuous pH indicator  
 272 assay, the conditions were as follows: [enzyme], 0-270 μg ml<sup>-1</sup>; [ester], 50 mM to ensure  
 273 substrate saturation; reaction volume, 44 μl; T, 30°C; and pH, 8.0. Abbreviations are as  
 274 follows: BFPME: benzoic acid, 4-formyl-, phenylmethyl ester; BHPP: benzyl (*R*)-2-hydroxy-3-

275 phenylpropanoate. LogP values and molecular volume of each ester were calculated using  
 276 ACD/ChemSketch 2015.2.5 and Molinspiration software, respectively. For raw data and  
 277 details, see Table S2.  
 278



279  
 280  
 281 **Fig. 3.** Chiral substrate specificity. The  $k_{cat}$  ( $s^{-1}$ ) values of the EH<sub>3</sub>, EH<sub>3I244L</sub> and EH<sub>3I244F</sub> variants  
 282 measured for 18 chiral carboxylic esters found to be hydrolyzed by any of the enzyme  
 283 variants. Abbreviations are as follows: E(R)CHB, ethyl (R)-4-chloro-3-hydroxybutyrate;  
 284 E(S)CHB, ethyl (S)-4-chloro-3-hydroxybutyrate. Figure preparation and experimental details  
 285 are shown in Fig. 2. The structures of methyl-(R)-2-phenylpropanoate and methyl-(S)-  
 286 phenylpropanoate used for soaking and investigation of chiral specificity are shown. LogP  
 287 values and the molecular volume of each ester were calculated using ACD/ChemSketch  
 288 2015.2.5 and Molinspiration software, respectively. For raw data and details, see Table S2.  
 289

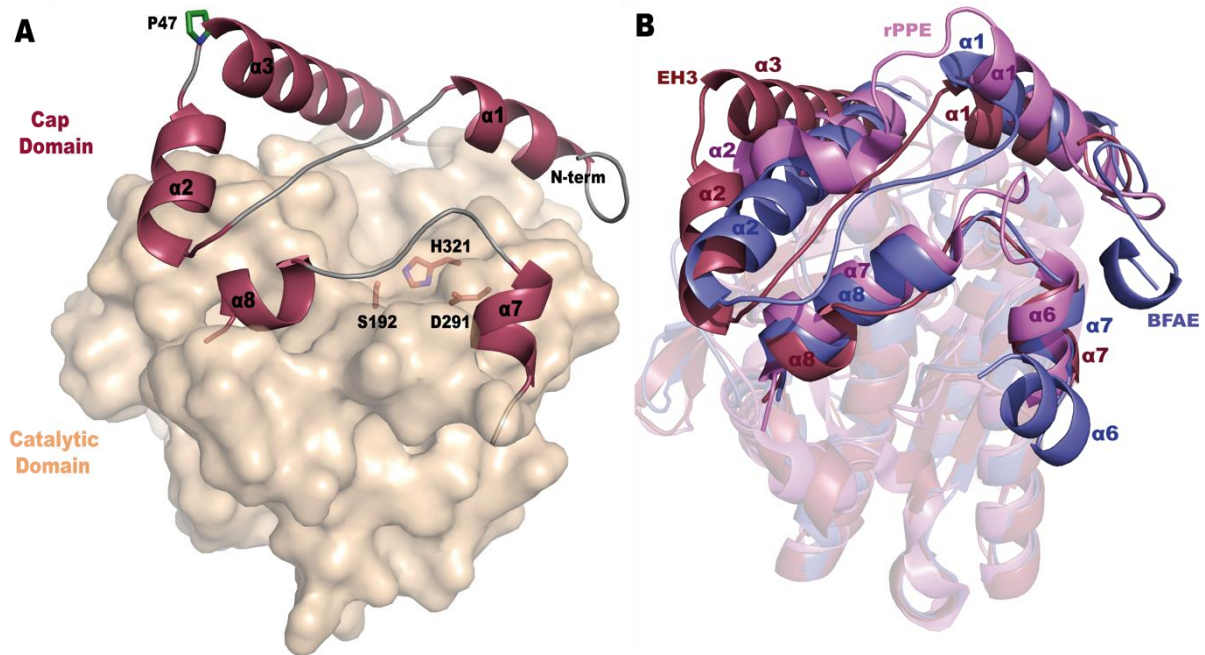
290 **Table 1.**  $E_{app}$  values for the hydrolysis of separate pairs of enantiomers.  
 291

Chiral pair (R/S)	$E_{app}$ : ( $k_{cat}/K_m$ preferred)/( $k_{cat}/K_m$ nonpreferred) <sup>1</sup>		
	EH <sub>3</sub>	EH <sub>3I244L</sub>	EH <sub>3I244F</sub>
Menthyl acetate	1.71±0.25 (S)	1.50±0.39 (S)	6.40±0.37 (S)
Methyl mandelate	1.53±0.24 (S)	1.93±0.15 (S)	3.24±0.04 (S)
Neomenthyl acetate	6.93±0.35 (R)	6.88±0.14 (R)	100% specific (R)
Methyl lactate	2.35±0.11 (R)	2.49±0.03 (R)	226.5±4.5 (R)
Ethyl lactate	1.74±0.16 (R)	1.76±0.21 (R)	9.03±0.91 (R)
Ethyl-4-chloro-3-hydroxybutyrate	1.59±0.18 (R)	1.39±0.05 (R)	6.22±0.28 (R)
Methyl-3-hydroxybutyrate	1.33±0.34 (R)	1.27±0.16 (R)	100% specific (R)
Methyl-3-hydroxyvalerate	1.02±0.10 (R)	1.09±0.14 (R)	100% specific (R)
Methyl-2-phenylpropanoate	2.21±0.08 (S)	2.16±0.05 (S)	56300±42 (S)

292 <sup>1</sup>Calculated by following the hydrolysis of separate enantiomers in a continuous high-  
 293 throughput pH indicator assay (see Materials and methods).  
 294

### 295 3.2 Insights into the structural basis of EH<sub>3</sub> substrate ambiguity

296 As previously reported by us [39], the crystal structure of EH<sub>3</sub> showed that it is folded into  
 297 two different domains: an  $\alpha/\beta$ -hydrolase catalytic domain housing the catalytic triad (S192,  
 298 A291, and H321) and a cap domain located on top and preventing the entrance of substrates  
 299 into the active site (**Fig. 4A**). The polypeptide chain is folded into a total of eleven  $\alpha$ -helices  
 300 and eight  $\beta$ -sheets; five of the  $\alpha$ -helices compose the cap domain, three at the N-terminus  
 301 ( $\alpha$ 1,  $\alpha$ 2,  $\alpha$ 3) and two more ( $\alpha$ 7 and  $\alpha$ 8) after strand  $\beta$ 6 from the central sheet (**Fig. S1**). The  
 302 analysis of the B factor values revealed that the cap region comprising  $\alpha$ 1- $\alpha$ 2 is highly  
 303 flexible, with the loop linking both  $\alpha$ -helices being partially disordered in the native structure  
 304 but becoming more ordered upon substrate binding.  
 305



306  
 307  
 308 **Fig. 4.** Crystal structure of EH<sub>3</sub>. (A) Molecular surface of the catalytic domain (wheat) with  
 309 the  $\alpha$ -helices making up the cap domain depicted as a cartoon (plum); for secondary  
 310 structure numbering, see **Fig. S1**. The catalytic triad is shown as sticks (orange). The region  
 311 comprising  $\alpha$ 1- $\alpha$ 2 is highly flexible, and P47 acts as a hinge (green sticks). (B)  
 312 Superimposition of the EH<sub>3</sub> subunit (plum) and its homologues, BFAE (slate, PDB ID: 1JKM)  
 313 and rPPE<sub>S159A/W187H</sub> (violet, PDB ID: 4OB6). The cap domain presents the largest differences  
 314 that configure markedly divergent active sites. The folding characteristics of Est22 and Est25  
 315 are most similar to those of EH<sub>3</sub> and BFAE, respectively, and have been omitted for clarity.  
 316

317 To disclose the molecular basis behind the substrate ambiguity, we compared the EH<sub>3</sub>  
 318 structure with other reported esterases. As expected, this highly flexible cap is the most  
 319 variable region among homologues. Analysis of EH<sub>3</sub> folding using the *DALI* server shows that  
 320 its closest homologue is Est22, which was isolated from environmental samples, with 64%  
 321 identity and an RMSD of 0.9 Å from 336 C $\alpha$  atoms [51] (PDB ID: 5HC0). Other homologues  
 322 are Est25 from environmental samples (RMSD of 1.8 Å from 323 C $\alpha$  atoms, PDB ID: 4J7A  
 323 [52]), Brefeldin A (BFAE) from *Bacillus subtilis* (RMSD of 2.0 Å from 323 C $\alpha$  atoms, PDB ID:  
 324 1JKM [53]) and the carboxylesterase rPPE from *Pseudomonas putida* (RMSD of 2.0 Å from  
 325 297 C $\alpha$  atoms, PDB ID: 4OB6 [54]), and these three proteins are 20-40% identical to EH<sub>3</sub>.  
 326 They all belong to the hormone-sensitive lipase (HSL) family or family IV [31]. This HSL family

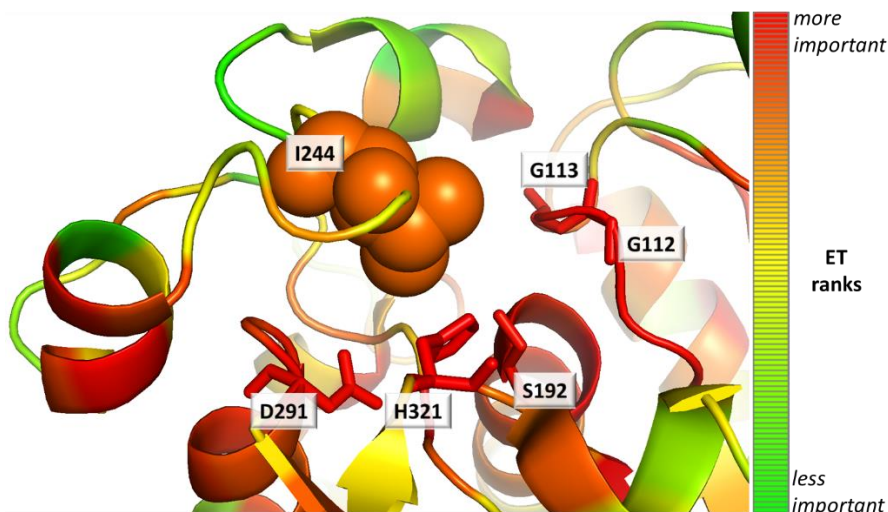
327 presents a very conserved folding at the core  $\alpha/\beta$  domain, with the largest differences at the  
328 cap domain that, consequently, must be mostly responsible for their different functionalities  
329 (**Fig. 4B**). First, the loop connecting helices  $\alpha1$  and  $\alpha2$  is very short in rPPE, and as a result,  
330 the active site cavity of this protein is reduced, allowing relatively small substrates to enter.  
331 Moreover, the EH<sub>3</sub> and Est22  $\alpha2$  and  $\alpha3$  helices are fused into a unique long  $\alpha$ -helix in BFAE  
332 and Est25. Although this arrangement in two separate, more mobile helices is shared with  
333 Est22, EH<sub>3</sub> presents a proline residue at the beginning of  $\alpha3$  (P47, but this residue is a  
334 glutamate in Est22), which could act as a hinge to increase the mobility of the EH<sub>3</sub>  $\alpha1$ - $\alpha2$   
335 moiety (**Fig. 4A**). This feature might be an additional mechanism that adapts the topology of  
336 the EH<sub>3</sub> active site to a higher variety of substrates and explains its observed substrate  
337 promiscuity. Furthermore, the shorter  $\alpha8$  in EH<sub>3</sub> makes a longer  $\alpha7$ - $\alpha8$  loop and a wider  
338 catalytic site, probably also contributing to the superior substrate promiscuity of EH<sub>3</sub>.  
339 Moreover, as a homologous HSL enzyme, EH<sub>3</sub> is a homodimer where both subunits are  
340 related by a twofold symmetry axis (**Fig. S2, Table S3**).

341 To conclude, EH<sub>3</sub> may be considered a moderately thermostable serine ester hydrolase  
342 with prominent substrate ambiguity but is not stereospecific. This is the result of its novel  
343 capacity to adapt the topology of the large but occluded active site to a high variety of  
344 substrates.

### 346 3.3. Evolutionary screening of specificity swapping positions

347 To explore the functional roles of sequence positions, we used the Evolutionary Trace (ET)  
348 method [36,37]. In previous work [38], ET identified few key sequence positions that were  
349 able to alter the substrate specificity of homologous proteins; therefore, we hypothesized  
350 that ET would also be able to identify positions that modulate enzyme specificity in  
351 combination with substrate promiscuity. According to the ET ranks for the EH<sub>3</sub> protein  
352 (shown in **Table S4**), position 244 was ranked within the top 12% of residues, and it is the  
353 most important residue of the loop formed by residues 240-249 (loop  $\alpha7$ - $\alpha8$  at the cap, **Fig.**  
354 **4A**), which are in contact with the catalytic triad (**Fig. 5**).

355



356

357 **Fig. 5.** Evolutionary trace ranks for the EH<sub>3</sub> protein. The analysis used 410 homologous  
358 sequences of EH<sub>3</sub> with sequence identity as low as 20%. The ET ranks are represented on the  
359 structure with a color scale (the most important residues are red, and the least important  
360 residues are green). While the catalytic residues were ranked within the top most important  
361 residues (S192 was 3%, D291 was 2%, and H321 was 1%), residue I244 was ranked in the top

362 12%, and it was the most important residue of loop 240-249 in contact with the catalytic  
 363 residues. The figure was generated using the PDB structure 6SXP, PyMOL (version 1.8), ET  
 364 (with the position-specific option), and the PyMOL ET viewer [55].  
 365

366 Leucine and isoleucine are amino acids that are most commonly present (*ca.* 70% of the  
 367 closest homologous sequences) at position 244, as shown in the alignment, while other  
 368 amino acids, such as tryptophan and valine, appear less frequently and mostly in distant  
 369 homologs (**Table 2**). This was also confirmed when we used BLAST to search for the EH<sub>3</sub>  
 370 sequence in the nonredundant (nr) [56], UniProt [57], and Marref, MarDB and MarCat [58]  
 371 databases. We were able to report up to 10,000 alignment hits with a minimum query  
 372 coverage of 50% and an e-value cutoff of 1e<sup>-10</sup>, ensuring in all cases the correct alignment of  
 373 the three residues forming the catalytic triad (S192, D291, and H321), the two residues  
 374 (G112 and G113) forming the so-called oxyanion hole-stabilizing substrates, and the residue  
 375 (P47) acting as a hinge that allows mobility of the cap domain to control substrate access to  
 376 the catalytic site. Above an identity of 50%, all homologues contain either isoleucine (top  
 377 homologue WP\_156780860.1; identify, 67%; e-value, 3e<sup>-176</sup>) or leucine (top homologue  
 378 AKJ87259.1; identify, 66%; e-value, 7e<sup>-168</sup>), while TNF86759.1 (identify 67%; e-value 3e<sup>-169</sup>)  
 379 contains a methionine, and E3QWZ9 (identify 35%; e-value 2e<sup>-45</sup>) contains a phenylalanine  
 380 (**Table 2**). Variability at this position was only found to a higher extent at identities below  
 381 39.38% and e-values above 2.62 × 10<sup>-69</sup> (**Table 2**).  
 382

383 **Table 2.** Frequency of amino acids at position I244 (following EH<sub>3</sub> numeration) in EH<sub>3</sub>-  
 384 homologous proteins as detected by ET analysis and the top homologs.  
 385

AA at 244 <sup>1</sup>	Frequency (%) <sup>1</sup>	Top homologs		
		Accession number	Identity (%)	E-value
L	63.08	AKJ87259.1 <sup>2</sup>	66.00	7.00 × 10 <sup>-168</sup>
W	19.56	MBE82488.1 <sup>3</sup>	32.49	1.32 × 10 <sup>-30</sup>
I	8.07	WP_156780860.1 <sup>2</sup>	67.00	3.00 × 10 <sup>-176</sup>
V	3.18	HAY66678.1 <sup>3</sup>	40.78	8.13 × 10 <sup>-66</sup>
N	2.20	WP_042512518.1_MMP04251492 <sup>3</sup>	31.35	2.80 × 10 <sup>-23</sup>
T	0.98	GCA_002427755.1 <sup>3</sup>	32.18	5.84 × 10 <sup>-31</sup>
F	0.73	E3QWZ9 <sup>1</sup>	35.00	2.00 × 10 <sup>-45</sup>
A	0.49	WP_073577520.1 <sup>3</sup>	33.42	5.14 × 10 <sup>-53</sup>
H	0.49	POP51947.1_MMP08281192 <sup>3</sup>	31.23	1.34 × 10 <sup>-21</sup>
M	0.49	TNF86759.1 <sup>2</sup>	67.00	3.00 × 10 <sup>-169</sup>
G	0.24	MMP491463_308377 <sup>3</sup>	38.18	2.47 × 10 <sup>-56</sup>
P	0.24	WP_071722916.1_MMP05231544 <sup>3</sup>	30.15	6.93 × 10 <sup>-23</sup>
S	0.24	GCA_002389675.1 <sup>3</sup>	32.05	4.22 × 10 <sup>-27</sup>

386 <sup>1</sup>As a default, the server uses the UniRef90 database. This database was created after  
 387 filtering out sequences so that it does not contain duplicates or similar sequences (higher  
 388 sequence identity than 90%) among its members. This makes it a good source to find "more  
 389 representative" full-length sequences (fragments and short sequences were removed) of the  
 390 protein family evolution and indeed results in better ET accuracy than using more sequences  
 391 from other databases. The BLAST option for sequence identity was 20% (min.) to 95% (max.).  
 392 The e-value cutoff was 0.05, and up to 500 sequences were selected (above this number of

393 representative sequences, the ET scores no longer improved). Based on these results, the  
394 different amino acids (AAs) found at position 244 (following EH<sub>3</sub> numbering) are given.

395 <sup>2</sup>nr database (<https://blast.ncbi.nlm.nih.gov>)

396 <sup>3</sup>Other databases: UniProt (<https://www.uniprot.org/>) and MAR

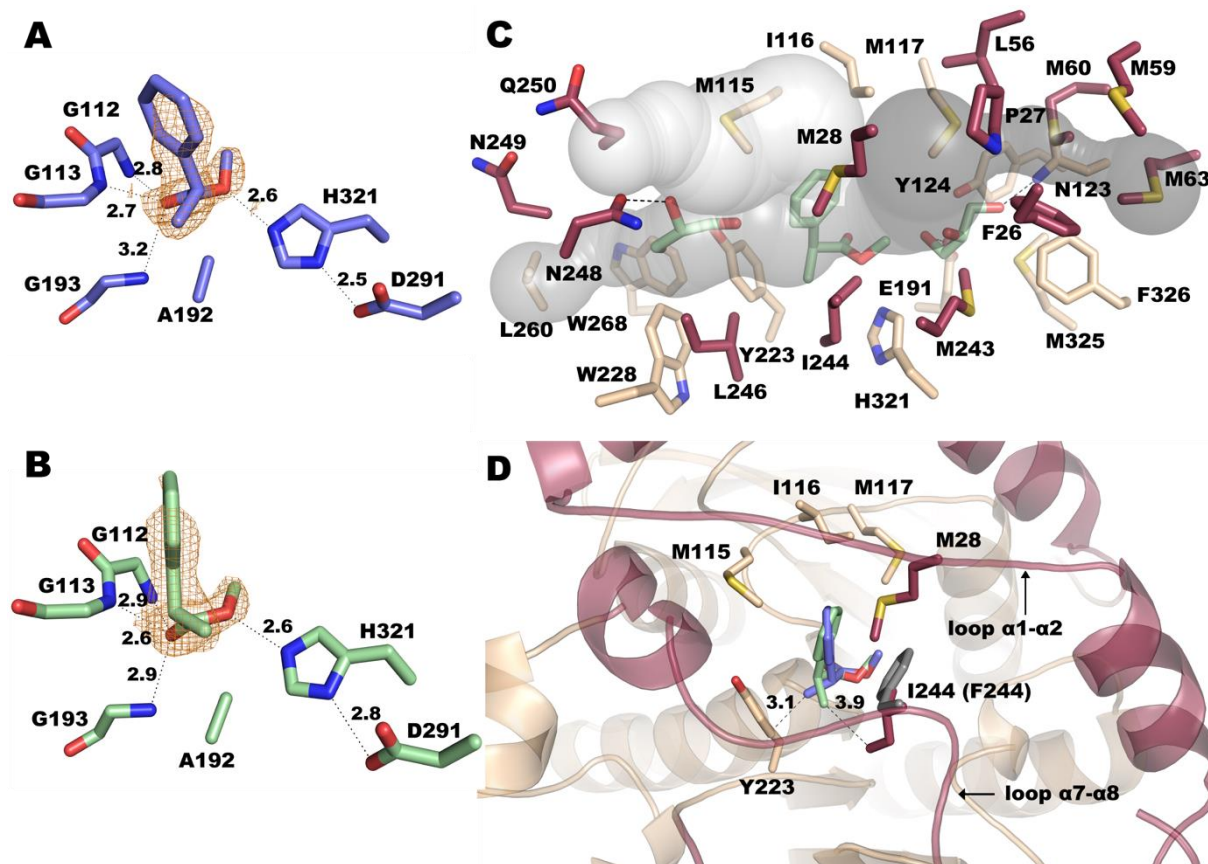
397 (<https://mmp.sfb.uit.no/blast/>).

398

### 399 3.4. Crystal structure of the substrate-bound form of EH<sub>3</sub> to determine the functional role of 400 I244

401 Our evolutionary trace analysis suggested that a single residue at position 244 potentially  
402 had a functionally important role in EH<sub>3</sub>. Soaking of inactivated EH<sub>3S192A</sub> crystals in a solution  
403 containing either methyl-(*R*)-2-phenylpropanoate or methyl-(*S*)-2-phenylpropanoate was  
404 performed in this study to further investigate whether I244, or other amino acid residue(s) if  
405 any, is close to the substrate's stereo-center and plays a functional role in specificity, as  
406 suggested by ET analysis. This chiral ester was selected as a model because it is structurally  
407 similar to ibuprofen-like esters that are of great industrial relevance, and the wild-type  
408 enzyme showed a lack of specificity for these chiral esters based on the  $E_{app}$  value (**Table 1**).  
409 The crystal structures of these complexes were solved using the coordinates of wild-type EH<sub>3</sub>  
410 (PDB ID: 6SXP). The final models were refined to crystallographic R-factors of 0.2100 and  
411 0.1919 and R-free values of 0.2403 and 0.2276 with resolutions of 2.27 and 2.06 Å (PDB IDs:  
412 6SYA and 6SXY), respectively. Both crystals present two molecules in the asymmetric unit  
413 forming the dimer and one ligand bound per catalytic site (**Figs. 6A and 6B**).

414



415

416

417 **Fig. 6.** Active site of EH<sub>3</sub>. **(A)** Methyl (*2R*)-2-phenylpropanoate and **(B)** methyl (*2S*)-2-  
418 phenylpropanoate bound at the catalytic site of EH<sub>3S192A</sub>, showing that the 2Fo-Fc electron

419 density maps contoured at 0.9 and 0.8  $\sigma$  are in orange. (C) Active site channels of EH<sub>3S192A</sub>, as  
420 calculated by CAVER [59], with bound methyl (2S)-2-phenylpropanoate and two glycerol  
421 molecules. The residues surrounding each cavity are shown. (D) Nearest environment and  
422 conserved binding mode of methyl (2R)-2-phenylpropanoate (slate) and methyl (2S)-2-  
423 phenylpropanoate (pale green) in the complexes; the closest distance from each substrate to  
424 the EH<sub>3</sub> residue is shown. The putative position of the modeled I244F mutant is shown as  
425 gray sticks. Panels C and D show the same color code as Fig. 4A.  
426

427 The catalytic triad of EH<sub>3</sub> is formed by S192, D291 and H321. There are three conserved  
428 motifs in its sequence, <sup>110</sup>HGGG<sup>113</sup> (containing two of the glycines involved in the oxyanion  
429 hole), the pentapeptide <sup>190</sup>GXSXG<sup>194</sup> (housing the nucleophile serine and a third glycine) and  
430 <sup>291</sup>DPLRDEG<sup>297</sup> (including D291). The substrates are bound by polar interactions of its free  
431 carboxylate oxygen with the three glycines forming the oxyanion hole and hydrogen bonds  
432 of the ester oxygen to H321 from the catalytic triad (Figs. 6A and 6B). Structural  
433 superimposition of the wild-type coordinates with the complexes presented here shows no  
434 structural changes in the EH<sub>3</sub> active site upon complex formation, and both complexes  
435 maintain high B factor values for the cap domain. As we previously described, the EH<sub>3</sub> active  
436 site cavity possesses three long channels giving access to catalytic S192, an acyl binding site  
437 (approximately 11.2 Å), an alcohol binding site (10.9 Å) and a third channel that can possibly  
438 allocate substrates with branched acyls (Fig. 6C). In the complex reported here, the acyl  
439 channel is partially occupied by phenyl/methyl rings, whereas the alcohol binding channel is  
440 allocated to a small aliphatic group (methyl). Chain B from both complexes also  
441 accommodates two molecules of glycerol coming from the cryoprotectant, one at the acyl  
442 moiety and the other at the alcohol site. As seen in Fig. 6C, all three channels are shaped by  
443 mostly hydrophobic residues from the cap and the catalytic domains that, in principle, would  
444 not present specific interactions with the substrates, explaining the EH<sub>3</sub> promiscuity and  
445 absence of stereospecificity. Thus, residues M115, Y223, W228, L246, I244 and L260  
446 protrude at the acyl channel, making a mostly hydrophobic tunnel where only N248 seems  
447 able to make polar interactions with the trapped glycerol molecule. In the alcohol channel,  
448 hydrophobic residues F26, L56, M59, M60 and M63 emerge, among others, and only two  
449 polar residues, N123 and E191, form hydrogen bonds with the glycerol trapped within this  
450 channel.

451 A close inspection of the substrate complexes reveals the main features of the binding  
452 modes of both isomers (Fig. 6D). Keeping the same polar interactions at the carboxylate  
453 ester moiety shown in Figs. 6A and 6B, the orientation of their bulky phenyl ring is slightly  
454 adjusted in a hydrophobic pocket surrounded by M115-I116-M117 from the catalytic  
455 domain and M28 from the cap  $\alpha$ 1- $\alpha$ 2 loop. The position of the aromatic ring is tilted in this  
456 pocket in the proper way that minimizes the steric hindrance of the methyl group to the  
457 closest residues, Y223 (in the *R* isomer) or I244 (in the *S* isomer), both delineating the  
458 proximal region of the acyl channel. Therefore, in principle, these two positions may be  
459 potential candidates to introduce the binding preferences of the isomers. However, changes  
460 in Y223, which is tightly fixed by the interaction with W228 and W268, as seen in Fig. 6C,  
461 might be deleterious for the active site integrity. This, together with the fact that Y223 was  
462 found to be less important than I244 (cap domain) according to evolutionary traces (most  
463 important 32%), similar to its interacting tryptophans (W228 and W268 were most  
464 important 57% and 22%, respectively), was the basis by which we concentrated our efforts

465 on I244. Its close proximity to the substrates and its prominent position at the long  $\alpha 7$ - $\alpha 8$   
466 loop suggest a crucial role in binding specificity.

467 To conclude, our structural analysis of the chiral substrate-bound form of inactivated  
468 protein has provided new information explaining the broad substrate promiscuity of EH<sub>3</sub>,  
469 which could not be observed previously by examining the crystal structure in free form [39].  
470 Indeed, the results imply that three long channels exist and give access to the catalytic  
471 nucleophile, which may then also contribute to the prominent substrate ambiguity of EH<sub>3</sub>  
472 and to its capacity to accept a large variety of esters with different sizes and degrees of  
473 conformational dynamics without chiral specificity. In addition, it has also contributed to  
474 confirming position 244 as a key position possibly influencing chiral specificity, thus  
475 supporting ET prediction.

### 476 477 *3.5. Position 244 introduces chiral specificity without major influences on substrate* 478 *ambiguity*

479 To choose which amino acid substitutions of residue I244 to study experimentally, in  
480 addition to evolutionary trace analysis, BLAST and structure analyses, we used the  
481 Evolutionary Action (EA) method. EA estimates the functional impact of each mutation in a  
482 protein and ranks the variants on a scale from 0 (fully neutral) to 100 (fully deleterious) [48],  
483 while variants with intermediate scores (e.g., between 40 and 70) have been linked with the  
484 partial loss or gain of function. In search of gain-of-function effects, we decided to perform  
485 two mutations: I244L, which has an EA score of 47 and appears in many homologous  
486 sequences (identity up to 66%), and I244F, which is a large amino acid, has an EA score of *ca.*  
487 64, and appears only in distant homologs (E3QWZ9-1, 35% identity as top hit) (**Table 3**).

488  
489 **Table 3. EA scores for mutations in position I244 of EH<sub>3</sub>.**  
490

Substitution	Evolutionary Action
I244V	37.83
I244L	46.94
I244M	47.51
I244F	63.58
I244Y	75.39
I244C	75.51
I244T	75.83
I244A	80.26
I244W	81.50
I244N	88.04
I244S	88.93
I244Q	89.28
I244P	89.47
I244H	90.50
I244R	92.53
I244G	93.95
I244K	95.10
I244E	96.97
I244D	97.55

491

492 The EH<sub>3I244L</sub> and EH<sub>3I244F</sub> variants were created by site-directed mutagenesis, and after  
493 expression in the pBXNH3 plasmid and *E. coli* MC1061 cells, the mutants were expressed,  
494 purified and characterized using the same protocols as those for the wild-type hydrolase  
495 following the hydrolysis of 98 carboxylic ester substrates. Their overall substrate spectra,  
496 maximum conversion rates and preferences for chiral esters were evaluated and compared  
497 with those of the wild-type protein.

498 As shown in **Figs. 2** and **3**, EH<sub>3</sub> can transform as many as 71 substrates, including chiral  
499 and non-chiral substrates, with the highest  $k_{cat}$  of 1730.3 min<sup>-1</sup>; these features were also  
500 characteristic of the EH<sub>3I244L</sub> mutant capable of hydrolyzing the same set of substrates (**Figs.**  
501 **2** and **3**) at similar rates (highest  $k_{cat}$  of 1731.3 min<sup>-1</sup>); indeed, the differences in  $k_{cat}$  for the  
502 conversion of each ester ranged only from *ca.* 0.7- to 3.2-fold, which suggests no major  
503 effects of the mutation on the substrate specificity and conversion rate. The substrate  
504 spectrum of EH<sub>3I244F</sub> was slightly reduced to 53 substrates (**Figs. 2** and **3**); many large  
505 substrates could not be hydrolyzed (such as long alkyl esters or paraben esters), but small  
506 substrates such as vinyl acetate and butyrate or propyl propionate and butyrate could be  
507 hydrolyzed. Furthermore, when compared to those of the wild type, the  $k_{cat}$  values of  
508 EH<sub>3I244F</sub> appeared to be lower for most substrates converted, with an average reduction of  
509 *ca.* 2.21 (interquartile range from 9.35 to 1.24) and a maximal reduction up to 992-fold (for  
510 methyl (*R*)-2-phenylpropanoate). Conversion only increased by *ca.* 2.9-fold for methyl (*S*)-2-  
511 phenylpropanoate. These reductions in the substrate repertoire and the conversion rate can  
512 be reasonably attributed to the incorporation of a large amino acid residue that does not  
513 accommodate as many substrates as wild-type EH<sub>3</sub> and mutant EH<sub>3I244L</sub>.

514 Strikingly, the analysis of the  $k_{cat}$  values of separate enantiomers within a series of nine  
515 chiral ester couples further revealed significant differences in the preference for chiral esters  
516 (**Fig. 3**). This is exemplified by the apparent significant preference of the EH<sub>3I244F</sub> mutant for  
517 methyl (*S*)-2-phenylpropanoate, (1*R*)-neomethyl acetate, methyl (*S*)-3-hydroxybutyrate, and  
518 methyl (*S*)-3-hydroxyvalerate compared to their chiral partners. This contrasts with the wild-  
519 type EH<sub>3</sub> and the EH<sub>3I244L</sub> mutant, which display no apparent preference for any of the chiral  
520 pairs (**Fig. 3**). As shown in **Table 1**, the  $E_{app}$  values of EH<sub>3</sub> and mutant EH<sub>3I244L</sub> ranged from  
521 1.02±0.10 to 6.93±0.35 and from 1.04±0.14 to 6.88±0.14, respectively. In contrast, EH<sub>3I244F</sub>  
522 hydrolyzed (1*R*)-neomethyl acetate, methyl (*S*)-3-hydroxybutyrate, and methyl (*S*)-3-  
523 hydroxyvalerate, with no appreciable hydrolysis of the other enantiomers detected with our  
524 assay conditions, and showed high preferences for methyl (*R*)-lactate ( $E_{app}$ : *ca.* 227±5) and  
525 methyl-(*S*)-2-phenylpropanoate ( $E_{app}$ : *ca.* 56300±42) (**Table 1**); these values are above  $E_{app}$  >  
526 25, indicative of interest for industrial applications [39].

527 Encouraged by these promising results, we carried out additional kinetic analyses with  
528 separate methyl-2-propanoate enantiomers used for soaking experiments and confirmed  
529 the absence of preferences of EH<sub>3</sub> and EH<sub>3I244L</sub> at any incubation time (**Fig. S3**) and the  
530 marked preference of EH<sub>3I244F</sub> for methyl-(*S*)-2-phenylpropanoate. These results were  
531 confirmed by measuring the enantiomeric excess (*e.e.*%) with a racemic mixture of methyl-2-  
532 propanoate enantiomers by GC [22], with values of 99.99±0.35% for EH<sub>3I244F</sub>, 41.70±0.48%  
533 for EH<sub>3</sub> and 42.5±0.44% for EH<sub>3I244L</sub>.

534 Collectively, EH<sub>3</sub> gained stereospecificity properties in the I244F mutant. This increase can  
535 be explained by the presence of a bulky residue that impedes the binding or positioning of  
536 one of the enantiomers. In the case of the methyl-2-phenylpropanoate substrate, for  
537 instance, both isomers could be able, in principle, to properly stack their phenyl moiety  
538 against the aromatic F244 side chain (**Fig. 6D**), but then the (*R*) isomer would probably

539 present high steric hindrance of its methyl group to the Y223 side chain, resulting in a  
540 preference for methyl-(*S*)-2-phenylpropanoate binding.

541

#### 542 **4. Conclusions**

543 Although multiple lines of evidence indicate a general trend of enzymes evolving from a  
544 generalist ancestor that accepts a broad range of substrates to a specialist enzyme [4], to  
545 our knowledge, there is no information on the coevolution of multi-specificity and chiral  
546 specificity. Here, combined analyses of specificity through evolutionary trace, structure  
547 determination and mutagenesis reveal that substrate ambiguity and chiral specificity in a  
548 single hydrolase can be modulated by a single residue. In this way, it is feasible to engineer  
549 prominent substrate-promiscuous yet stereospecific hydrolases that are relevant to the field  
550 of organic synthesis. We hypothesize that the number of enzymes with such characteristics  
551 will increase in the future through screening evolutionarily important single sequence  
552 positions, allowing us to swap substrate ambiguity and chiral specificity.

553

#### 554 **5. Accession number**

555 The coordinates and structure factors of EH<sub>3S192A</sub> complexed with methyl-(*R/S*)-2-  
556 phenylpropanoate have been deposited in the Protein Data Bank with the accession codes  
557 6SYA and 6SXY.

558

#### 559 **CRedit authorship contribution statement**

560 **Isabel Cea-Rama:** Methodology, Formal analysis. **Cristina Coscolín:** Methodology, Formal  
561 analysis. **Panagiotis Katsonis:** Methodology, Formal analysis. **Rafael Bargiela:** Formal  
562 analysis. **Peter N. Golyshin:** Methodology, Funding acquisition. **Olivier Lichtarge:**  
563 Methodology, Funding acquisition. **Manuel Ferrer:** Formal analysis, Resources, Writing –  
564 original draft, Funding acquisition. **Julia Sanz-Aparicio:** Formal analysis, Resources, Writing –  
565 original draft, Funding acquisition.

566

#### 567 **Declaration of Competing Interests**

568 The authors declare that they have no known competing financial interests or personal  
569 relationships that could have appeared to influence the work reported in this paper.

570

#### 571 **Acknowledgments**

572 MF acknowledges the grant 'INMARE' from the European Union's Horizon 2020 (grant  
573 agreement no. 634486), the grants PCIN-2017-078 (within the Marine Biotechnology ERA-  
574 NET) and BIO2017-85522-R from the Ministerio de Economía, Industria y Competitividad,  
575 Agencia Estatal de Investigación (AEI), Fondo Europeo de Desarrollo Regional (FEDER) and  
576 the European Union (EU), and the grant 2020AEP061 from the Agencia Estatal CSIC. J.S.-A.  
577 acknowledges grant PID2019-105838RB-C33 from the Ministerio de Ciencia e Innovación,  
578 Agencia Estatal de Investigación (AEI), Fondo Europeo de Desarrollo Regional (FEDER) and  
579 the European Union (EU). P.N.G. acknowledges the support of the Era-Net IB Project  
580 MetaCat funded through UK Biotechnology and Biological Sciences Research Council  
581 (BBSRC), grant No. BB/M029085/1, and the Centre for Environmental Biotechnology Project,  
582 co-funded by European Regional Development Fund (ERDF) via the Welsh Government  
583 (WEFO); R.B. acknowledges the Supercomputing Wales project, co-funded by ERDF via  
584 WEFO. OL and PK were supported by the National Institutes of Health (NIH) grants  
585 5R01AG061105, 5R01GM066099, and 5R01GM079656. C. Coscolín thanks the Ministerio de

586 Economía y Competitividad and FEDER for a PhD fellowship (Grant BES-2015-073829). The  
587 authors would like to acknowledge David Rojo and Coral Barbas for GC analyses and David  
588 Almendral and Ruth Matesanz for CD analyses. We thank the staff of the Synchrotron  
589 Radiation Source at Alba (Barcelona, Spain) for assistance at the BL13-XALOC beamline.

590

## 591 **Appendix A. Supplementary data**

592 Supplementary data for this article can be found online.

593

## 594 **References**

595

- 596 [1] Jegannathan KR, Nielsen PH (2013) Environmental assessment of enzyme use in industrial  
597 production – a literature review. *J Clean Prod* 42: 228-240.
- 598 [2] Sheldon RA, Woodley JM (2018) Role of biocatalysis in sustainable chemistry. *Chem Rev* 118:  
599 801-838.
- 600 [3] Ferrer M, Méndez-García C, Bargiela R, Chow J, Alonso S, et al. (2020) Decoding the ocean's  
601 microbiological secrets for marine enzyme biodiscovery. *FEMS Microbiol Lett* 366: fny285.
- 602 [4] Tawfik DS, Gruic-Sovulj I (2020). How evolution shapes enzyme selectivity - lessons from  
603 aminoacyl-tRNA synthetases and other amino acid utilizing enzymes. *FEBS J* 287: 1284-1305.
- 604 [5] Coscolín C, Martínez-Martínez M, Chow J, Bargiela R, García-Moyano A, et al. (2018)  
605 Relationships between substrate promiscuity and chiral selectivity of esterases from  
606 phylogenetically and environmentally diverse microorganisms. *Catalysts* 8: 10.
- 607 [6] Arnold FH (2019) Innovation by evolution: Bringing new chemistry to life (Nobel lecture). *Angew*  
608 *Chem Int Ed Engl* 58: 14420-14426.
- 609 [7] Suplatov D, Švedas V (2015) Study of functional and allosteric sites in protein superfamilies. *Acta*  
610 *Naturae* 7: 34-45.
- 611 [8] Berezovsky IN, Guarnera E, Zheng Z, Eisenhaber B, Eisenhaber F (2017) Protein function  
612 machinery: from basic structural units to modulation of activity. *Curr Opin Struct Biol* 42: 67-74.
- 613 [9] Martínez-Martínez M, Coscolín C, Santiago G, Chow J, Stogios PJ, et al. (2018) Determinants and  
614 Prediction of Esterase Substrate Promiscuity Patterns. *ACS Chem Biol* 13: 225-234.
- 615 [10] Alcaide M, Tornés J, Stogios, PJ, Xu X, Gertler C, et al. (2013) Single residues dictate the co-  
616 evolution of dual esterases: MCP hydrolases from the  $\alpha/\beta$  hydrolase family. *Biochem J* 454: 157-  
617 166.
- 618 [11] Cadet F, Fontaine N, Li G, Sanchis J, Ng Fuk Chong M, et al. (2028) A machine learning approach  
619 for reliable prediction of amino acid interactions and its application in the directed evolution of  
620 enantioselective enzymes. *Sci Rep* 8: 16757.
- 621 [12] Koudelakova T, Chovancova E, Brezovsky J, Monincova M, Fortova A, et al. (2011) Substrate  
622 specificity of haloalkane dehalogenases. *Biochem J* 435: 345-354.
- 623 [13] Purg M, Pabis A, Baier F, Tokuriki N, Jackson C, Kamerlin SC (2016) Probing the mechanisms for  
624 the selectivity and promiscuity of methyl parathion hydrolase. *Philos Trans A Math Phys Eng Sci*  
625 374: 20160150.
- 626 [14] Ramírez-Escudero M, Del Pozo MV, Marín-Navarro J, González B, Golyshin PN, et al. (2016)  
627 Structural and functional characterization of a ruminal  $\beta$ -glycosidase defines a novel subfamily  
628 of glycoside hydrolase family 3 with permuted domain topology. *J Biol Chem* 291: 24200-24214.
- 629 [15] Albesa-Jové D, Guerin ME (2016) The conformational plasticity of glycosyltransferases. *Curr Opin*  
630 *Struct Biol* 40: 23-32.
- 631 [16] Garrabou X, Macdonald DS, Wicky BIM, Hilvert D (2018) Stereodivergent evolution of artificial  
632 enzymes for the michael reaction. *Angew Chem Int Ed Engl* 57: 5288-5291.
- 633 [17] Ekroos M, Sjögren T (2006) Structural basis for ligand promiscuity in cytochrome P450 3A4. *Proc*  
634 *Natl Acad Sci USA* 103: 13682-13687.

- 635 [18] Zou T, Risso VA, Gavira JA, Sanchez-Ruiz JM, Ozkan SB (2015) Evolution of conformational  
636 dynamics determines the conversion of a promiscuous generalist into a specialist enzyme. *Mol*  
637 *Biol Evol* 32: 132-143.
- 638 [19] Gao S, Zhu S, Huang R, Li H, Wang H, Zheng G (2017) Engineering the enantio-selectivity and  
639 thermostability of a (+)- $\gamma$ -lactamase from *Microbacterium hydrocarbonoxydans* for kinetic  
640 resolution of vince lactam (2-azabicyclo[2.2.1]hept-5-en-3-one). *Appl Environ Microbiol* 84:  
641 e01780-17.
- 642 [20] Mateljak I, Monza E, Lucas MF, Guallar V, Aleksejeva O, et al. (2019) Increasing redox potential,  
643 redox mediator activity and stability in a fungal laccase by computer-guided mutagenesis and  
644 directed evolution. *ACS Catal* 9: 4561-4572.
- 645 [21] Wu Z, Kan SBJ, Lewis RD, Wittmann BJ, Arnold FH (2019) Machine learning-assisted directed  
646 protein evolution with combinatorial libraries. *Proc Natl Acad Sci USA* 116: 8852-8858.
- 647 [22] Alonso S, Santiago G, Cea-Rama I, Fernandez-Lopez L, Coscolín C, et al. (2020) Genetically  
648 engineered proteins with two active sites for enhanced biocatalysis and synergistic chemo- and  
649 biocatalysis. *Nat Catal* 3: 319-328.
- 650 [23] Park S, Morley KL, Horsman GP, Holmquist M, Hult K, et al. (2005) Focusing mutations into the P.  
651 *fluorescens* esterase binding site increases enantioselectivity more effectively than distant  
652 mutations. *Chem Biol* 12: 45-54.
- 653 [24] Lafaquière V, Barbe S, Puech-Guenot S, Guieysse D, Cortés J, et al. (2009) Control of lipase  
654 enantio-selectivity by engineering the substrate binding site and access channel. *Chembiochem*  
655 10: 2760-2771.
- 656 [25] Antipov E, Cho AE, Klivanov AM (2009) How a single-point mutation in horseradish peroxidase  
657 markedly enhances enantioselectivity. *J Am Chem Soc* 131: 11155-11160.
- 658 [26] Sevrioukova IF, Poulos TL (2013). Understanding the mechanism of cytochrome P450 3A4:  
659 recent advances and remaining problems. *Dalton Trans* 42: 3116-3126.
- 660 [27] Stenner R, Steventon JW, Seddon A, Anderson JLR (2020) A de novo peroxidase is also a  
661 promiscuous yet stereoselective carbene transferase. *Proc Natl Acad Sci USA* 117: 1419-1428.
- 662 [28] van der Meer JY, Poddar H, Baas BJ, Miao Y, Rahimi M, et al. (2016) Using mutability landscapes  
663 of a promiscuous tautomerase to guide the engineering of enantioselective Michaelases. *Nat*  
664 *Commun* 7: 10911.
- 665 [29] Risso VA, Gavira JA, Mejia-Carmona DF, Gaucher EA, Sanchez-Ruiz JM (2013) Hyperstability and  
666 substrate promiscuity in laboratory resurrections of Precambrian  $\beta$ -lactamases. *J Am Chem Soc*  
667 135: 2899-2902.
- 668 [30] Nobili A, Tao Y, Pavlidis IV, van den Bergh T, Joosten HJ, et al. (2015) Simultaneous use of in  
669 silico design and a correlated mutation network as a tool to efficiently guide enzyme  
670 engineering. *Chembiochem* 16: 805-810.
- 671 [31] Höppner A, Bollinger A, Kobus S, Thies S, Coscolín C, et al. (2020) Crystal structures of a novel  
672 family IV esterase in free and substrate-bound form. *FEBS J* Dec 20. doi: 10.1111/febs.15680.  
673 Epub ahead of print.
- 674 [32] Bauer TL, Buchholz PCF, Pleiss J (2020) The modular structure of alpha/beta-hydrolases. *FEBS J*  
675 287: 1035-1053.
- 676 [33] Studer RA, Dessailly BH, Orengo CA (2013) Residue mutations and their impact on protein  
677 structure and function: detecting beneficial and pathogenic changes. *Biochem J* 449: 581-594.
- 678 [34] Jack BR, Meyer AG, Echave J, Wilke CO (2016) Functional sites induce long-range evolutionary  
679 constraints in enzymes. *PLoS Biol* 14: e1002452.
- 680 [35] Guzmán GI, Sandberg TE, LaCroix RA, Nyerges Á, Papp H, et al. (2019). Enzyme promiscuity  
681 shapes adaptation to novel growth substrates. *Mol Syst Biol* 15: e8462.
- 682 [36] Lichtarge O, Bourne HR, Cohen FE (1996) An evolutionary trace method defines binding surfaces  
683 common to protein families. *J Mol Biol* 257: 342-358.
- 684 [37] Mihalek I, Res I, Lichtarge O (2004). A family of evolution-entropy hybrid methods for ranking  
685 protein residues by importance. *J Mol Biol* 336: 1265-1282.

- 686 [38] Rodriguez GJ, Yao R, Lichtarge O, Wensel TG (2010) Evolution-guided discovery and recoding of  
687 allosteric pathway specificity determinants in psychoactive bioamine receptors. *Proc Natl Acad*  
688 *Sci USA* 107: 7787-7792.
- 689 [39] Giunta CI, Cea-Rama I, Alonso S, Briand ML, Bargiela R, et al. (2020) Tuning the properties of  
690 natural promiscuous enzymes by engineering their nano-environment. *ACS Nano* 14: 17652-  
691 17664.
- 692 [40] Kabsch W (2010) XDS. *Acta Crystallogr D Biol Crystallogr* 66: 125-132.
- 693 [41] Evans PR, Murshudov GN (2013) How good are my data and what is the resolution? *Acta*  
694 *Crystallogr D Biol Crystallogr* 69: 1204-1214.
- 695 [42] Winn MD, Ballard CC, Cowtan KD, Dodson EJ, Emsley P, et al. (2011) Overview of the CCP4 suite  
696 and current developments. *Acta Crystallogr D Biol Crystallogr* 67: 235-242.
- 697 [43] Murshudov GN, Vagin AA, Dodson EJ (1997) Refinement of macromolecular structures by the  
698 maximum-likelihood method. *Acta Crystallogr D Biol Crystallogr* 53: 240-255.
- 699 [44] Emsley P, Lohkamp B, Scott WG, Cowtan K (2010) Features and development of Coot. *Acta*  
700 *Crystallogr D Biol Crystallogr* 66: 486-501.
- 701 [45] Moriarty NW, Grosse-Kunstleve RW, Adams PD (2009) Electronic Ligand Builder and  
702 Optimization Workbench (eLBOW): a tool for ligand coordinate and restraint generation. *Acta*  
703 *Crystallogr D Biol Crystallogr* 65: 1074-1080.
- 704 [46] Fraczkiwicz R, Braun W (1998) Exact and efficient analytical calculation of the accessible surface  
705 areas and their gradients for macromolecules. *J Comput Chem* 19: 319.
- 706 [47] Guilloux VL, Schmidtke P, Tuffery P (2009) Fpocket: An open source platform for ligand pocket  
707 detection. *BMC Bioinformatics* 10: 168.
- 708 [48] Katsonis P, Lichtarge O (2014) A formal perturbation equation between genotype and  
709 phenotype determines the Evolutionary Action of protein-coding variations on fitness. *Genome*  
710 *Res* 24: 2050-2058.
- 711 [49] Badger JH, Hoover TR, Brun YV, Weiner RM, Laub MT, et al. (2006) Comparative genomic  
712 evidence for a close relationship between the dimorphic prosthecate bacteria *Hyphomonas*  
713 *neptunium* and *Caulobacter crescentus*. *J Bacteriol* 188: 6841-6850.
- 714 [50] Janes LE, Kazlauskas RJ (1997) Quick E. A fast spectrophotometric method to ensure the  
715 enantioselectivity of hydrolases. *J Org Chem* 62: 4560-4561.
- 716 [51] Huang J, Huo YY, Ji R, Kuang S, Ji C, Xu XW, Li J (2016) Structural insights of a hormone sensitive  
717 lipase homologue Est22. *Sci Rep* 6: 28550.
- 718 [52] Ngo TD, Ryu BH, Ju H, Jang E, Park K, et al. (2013) Structural and functional analyses of a  
719 bacterial homologue of hormone-sensitive lipase from a metagenomic library. *Acta Crystallogr D*  
720 *Biol Crystallogr* 69: 1726-1737.
- 721 [53] Wei Y, Contreras JA, Sheffield P, Osterlund T, Derewenda U, et al. (1999). Crystal structure of  
722 brefeldin A esterase, a bacterial homolog of the mammalian hormone-sensitive lipase. *Nat*  
723 *Struct Biol* 6: 340-345.
- 724 [54] Dou S, Kong XD, Ma BD, Chen Q, Zhang J, et al. (2014) Crystal structures of *Pseudomonas putida*  
725 esterase reveal the functional role of residues 187 and 287 in substrate binding and chiral  
726 recognition. *Biochem Biophys Res Commun* 446: 1145-1150.
- 727 [55] Lua RC, Lichtarge O (2010) PyETV: A PyMOL evolutionary trace viewer to analyze functional site  
728 predictions in protein complexes. *Bioinformatics* 26: 2981-2982.
- 729 [56] Altschul SF, Gish W, Miller W, Myers EW, Lipman DJ (1990) Basic local alignment search tool. *J*  
730 *Mol Biol* 215: 403-410.
- 731 [57] UniProt Consortium (2019) UniProt: a worldwide hub of protein knowledge. *Nucleic Acids Res*  
732 47: D506-D515.
- 733 [58] Klemetsen T, Raknes IA, Fu J, Agafonov A, Balasundaram SV, et al. (2018) The MAR databases:  
734 development and implementation of databases specific for marine metagenomics. *Nucleic Acids*  
735 *Res* 46: D692-D699.

736 [59] Jurcik A, Bednar D, Byska J, Marques SM, Furmanova K, et al. (2018) CAVER Analyst 2.0: analysis  
737 and visualization of channels and tunnels in protein structures and molecular dynamics  
738 trajectories. *Bioinformatics* 34: 3586-3588.